Inside out and upside-down: The roles of gas cooling and dynamical heating in shaping the stellar age–velocity relation

Jonathan C. Bird [ORCID],[1]*† Sarah R. Loebman,[2,3]‡ David H. Weinberg,[4,5] Alyson M. Brooks,[6] Thomas R. Quinn[7] and Charlotte R. Christensen[8]

[1]*Department of Physics and Astronomy, Vanderbilt University, 6301 Stevenson Center, Nashville, TN 37235, USA*
[2]*Department of Physics, University of California, Merced, CA 95343, USA*
[3]*Department of Physics, University of California, Davis, 1 Shields Ave, Davis, CA 95616, USA*
[4]*Department of Astronomy, The Ohio State University, 140 West 18th Avenue, Columbus, OH 43210, USA*
[5]*Center for Cosmology and Astro-Particle Physics, The Ohio State University, 191 West Woodruff Avenue, Columbus, OH 43210, USA*
[6]*Department of Physics and Astronomy, Rutgers University, 136 Frelinghuysen Rd., Piscataway, NJ 08854, USA*
[7]*Department of Astronomy, University of Washington, Box 351580, Seattle, WA 98115, USA*
[8]*Physics Department, Grinnell College, 1115 8th Ave, Grinnell, IA, 50112, USA*

ABSTRACT

Kinematic studies of disc galaxies, using individual stars in the Milky Way or statistical studies of global disc kinematics over time, provide insight into how discs form and evolve. We use a high-resolution, cosmological zoom-simulation of a Milky Way-mass disc galaxy (h277) to tie together local disc kinematics and the evolution of the disc over time. The present-day stellar age–velocity relationship (AVR) of h277 is nearly identical to that of the analogous solar-neighbourhood measurement in the Milky Way. A crucial element of this success is the simulation's dynamically cold multiphase ISM, which allows young stars to form with a low velocity dispersion ($\sigma_{\rm birth} \sim 6 - 8\ {\rm km\,s^{-1}}$) at late times. Older stars are born kinematically hotter (i.e. the disc settles over time in an 'upside-down' formation scenario), and are subsequently heated after birth. The disc also grows 'inside-out', and many of the older stars in the present-day solar neighbourhood are present because of radial mixing. We demonstrate that the evolution of $\sigma_{\rm birth}$ in h277 can be explained by the same model used to describe the general decrease in velocity dispersion observed in disc galaxies from $z \sim 2$–3 to the present-day, in which the disc evolves in quasi-stable equilibrium and the ISM velocity dispersion decreases over time due to a decreasing gas fraction. Thus, our results tie together local observations of the Milky Way's AVR with observed kinematics of high z disc galaxies.

Key words: stars: kinematics and dynamics – ISM: kinematics and dynamics – Galaxy: evolution – galaxies: evolution – galaxies: ISM – stars: formation.

1 INTRODUCTION

With the advent of advanced spectroscopic and IFU surveys, the detailed kinematics and evolution of disc galaxies are now being studied in unprecedented detail (e.g. MaNGA, SAMI, KMOS$^{\rm 3D}$; Bryant et al. 2015; Bundy et al. 2015; Wisnioski et al. 2019). Locally, we can use present-day stellar kinematics to infer the past evolution of our Milky Way (MW) through Galactic Archeology, (e.g. Belokurov et al. 2018; Frankel et al. 2018, 2019). At higher redshift, large galaxy surveys are yielding results on the evolution of populations of galaxies over time (e.g. see the review by Glazebrook 2013). If the MW (and other local galaxies) kinematically evolve in a fashion similar to high z galaxies, then in principle results from these two epochs should be able to be explained within the same theoretical framework.[1]

Galaxies in the Local Group show a clear correlation between stellar age and velocity dispersion (Leaman et al. 2017), e.g. the MW (e.g. Nordström et al. 2004), M31 (Dorman et al. 2015; Bhattacharya et al. 2019), and M33 (Beasley et al. 2015). Observations in all of these galaxies show that the velocity dispersion, σ, increases with increasing stellar age. Locally, young stars are born dynamically cold (e.g. Stark & Brand 1989; Kuhn et al. 2019). The classic explanation for this age–velocity relation (AVR) is that it is an evolutionary sequence brought about by the diffusion of stellar orbits: stars have always formed in dynamically cold gas, but various gravitational scattering mechanisms steadily increase the random orbital energy as a stellar population ages (e.g. Wielen 1977; Lacey 1984; and chapter 8.4 of Binney & Tremaine 2008). The scattering sources might be Giant Molecular Clouds (GMCs; e.g. Spitzer & Schwarzschild 1951; Lacey 1984; Villumsen 1985), or spiral arms and bars (e.g. Carlberg & Sellwood 1985; Sellwood & Binney 2002; Minchev & Quillen 2006; Roškar et al. 2008; Loebman et al. 2011; Grand et al. 2016). An alternative explanation for the origin of the AVR is that older stars were born dynamically hotter in the past, but that the disc 'settles' and becomes progressively cooler as the star forming gas cools with time. The stars might be dynamically hotter in the past due to a

*★ E-mail: jonathan.bird@vanderbilt.edu
† Stevenson Fellow
‡ Hubble Fellow
[1] h277 is now publicly available in its entirety at https://nbody.shop/data.html

more active galaxy merger phase (Toth & Ostriker 1992; Quinn, Hernquist & Fullagar 1993; Brook et al. 2004; Martig, Minchev & Flynn 2014; Hu & Sijacki 2018; Buck et al. 2020) or due to the fact that gravitational turbulence is higher if the disc is more gas rich (Bournaud, Elmegreen & Martig 2009), or due to a higher star formation rate (SFR; e.g. Lehnert et al. 2014).

The MW presents the best opportunity to infer a detailed understanding of galaxy formation. Combining proper motions and distances from the *Gaia* survey with stellar properties from spectroscopic surveys yields full 6D kinematics for hundreds of thousands of stars in the MW's disc along with moderately precise ages (Sanders & Das 2018). Studies of the MW using these data suggest it is possible to recreate the observed AVR with dynamical heating of stars alone to ages of ~ 8 Gyr (Gustafsson et al. 2016; Yu & Liu 2018; Mackereth et al. 2019; Ting & Rix 2019). However, these results do not rule out any contribution from disc settling over that same time-span. In fact, it is clear that steady orbital heating cannot be solely responsible for the relatively high velocity dispersion of stars older than 8 Gyr (e.g. Lacey 1984; Sellwood 2014; Mackereth et al. 2019).

Observations of rotating disc galaxies out to $z \sim 3$ show increasing velocity dispersion with increasing redshift (e.g. Flores et al. 2006; Gnerucci et al. 2011; Kassin et al. 2012; Wisnioski et al. 2015; Mieda et al. 2016; Simons et al. 2016; Mason et al. 2017). In these studies, the typical tracer of σ is gas that has been heated by star formation (e.g. Hα or ionized oxygen; Epinat et al. 2009; Förster Schreiber et al. 2009; Lemoine-Busserolle et al. 2010). Notably, molecular and atomic gas show roughly the same evolution, albeit for fewer galaxies (e.g. Tacconi et al. 2013; Übler et al. 2019). Many of the kinematic measurements at high z are for galaxies more massive than the MW (especially at $z > 1$), yet disc settling has been found even for less-massive populations (Law et al. 2009; Kassin et al. 2012; Contini et al. 2016; Hirtenstein et al. 2019).

A number of simulators have examined the origin of the AVR and/or the formation of galaxy thin/thick discs. One trend that has become clear is that the results can be strongly dependent on the star formation parameters, which are commonly limited by the simulation resolution (House et al. 2011; Martig, Minchev & Flynn 2014; Kumamoto, Baba & Saitoh 2017). By definition, higher resolution simulations can capture higher density gas. As resolution increases, simulators can restrict star formation to occur in higher density gas that more closely resembles GMCs (e.g. Governato et al. 2010; Dutton et al. 2019). House et al. (2011) showed that the threshold density for star formation was the dominant parameter in setting the stellar velocity dispersion at birth, σ_{birth}. For simulations with a low star formation density threshold ($n \sim 0.1$ cm^{-3}) that are unable to resolve cold, dense gas, a dispersion floor is imposed on σ_{birth}, causing a number of simulations to have stars that maintain a steady σ_{birth} over 8–10 Gyr, and with little to no subsequent heating of the stellar populations after birth. However, with an increase in resolution and star formation threshold ($n \sim 1$–5 cm^{-3}), a different result has emerged: an 'Upside-Down' formation in which stars form with progressively lower σ_{birth} with time (Bird et al. 2013; Grand et al. 2016). Scattering processes can subsequently heat the orbits of stars, causing the older stars to contribute to the AVR in the solar neighbourhood (Brook et al. 2012; Bird et al. 2013; Aumer, Binney & Schönrich 2016; Grand et al. 2016; Ma et al. 2017).

The resulting AVRs of some simulated galaxies are very similar in slope and normalization to the MW AVR. However, the kinematics of the youngest stars are generally too hot relative to observations (e.g. House et al. 2011; Bird et al. 2013; Roškar, Debattista & Loebman 2013; Martig, Minchev & Flynn 2014; Grand et al. 2016), even when star formation thresholds with $n > 100$ cm^{-3} are achieved

(Buck et al. 2020; Sanderson et al. 2020). In this paper, we present the first cosmological simulation of a MW-mass disc galaxy that also reproduces the low σ_{birth} determined for the MW.

Meanwhile, high-resolution simulations have separately also been used to interpret the observed decline in σ in disc galaxies with time. In general, a higher σ_{birth} in the past is well-motivated on theoretical grounds. Several groups have found correlations between velocity dispersion and star formation fuelled by marginal stability of the disc (e.g. Bournaud & Elmegreen 2009; Krumholz, Dekel & McKee 2012; Forbes et al. 2014; Benincasa et al. 2016; Krumholz & Burkhart 2016; Nestingen-Palm et al. 2017; Orr et al. 2018; Orr, Hayward & Hopkins 2019). In this framework, gravitational instabilities drive turbulent motions, which then naturally regulate galaxies to be marginally stable. This model predicts a relation between the gas velocity dispersion and the surface density of the gas in the galaxy. When combined with the Schmidt–Kennicutt star formation relation, the gas surface density is also tied to the star formation rate (e.g. Green et al. 2014; Leroy et al. 2016; Semenov, Kravtsov & Gnedin 2016). If the disc is marginally stable, and it is assumed that gas (rather than stars) is the predominant component of the gravitational potential, the higher gas surface densities and gas fractions at higher redshift (e.g. Genzel et al. 2006; Daddi et al. 2010; Jones et al. 2010; Genzel et al. 2011; Glazebrook 2013; Tacconi et al. 2013; Popping et al. 2015; Krumholz & Burkhart 2016; Stott et al. 2016; Wiklind et al. 2019) should naturally lead to higher gas velocity dispersion. For more local galaxies, feedback from star-formation may also play a critical role in setting a dynamical 'floor' for the star-forming gas (e.g. Agertz et al. 2009; Faucher-Giguère, Quataert & Hopkins 2013; Stilp et al. 2013; Semenov, Kravtsov & Gnedin 2018; Orr, Hayward & Hopkins 2019; Orr et al. 2020). These models predict that σ_{birth} should be strongly correlated with the SFR. This correlation has been seen for the population of massive, rotating galaxies observed at high z (e.g. Swinbank et al. 2012; Wisnioski et al. 2015; Turner et al. 2017; Übler et al. 2019).

While observational works infer disc settling through population studies over redshift, simulators have examined the evolution of individual discs to trace the evolution in σ over time (Kassin et al. 2014; Ceverino et al. 2017; Hung et al. 2019). In all cases, cosmological zoom simulations of individual disc galaxies show a decrease in gas velocity dispersions since $z \sim 1.5$, consistent with observations. Kassin et al. (2014) used four MW-mass simulations (one of which is used in this paper) to demonstrate that individual simulated discs show the same slope of gas velocity dispersion versus z as observations, but they did not investigate the origin of the trend. Likewise, Hung et al. (2019) attempted to measure gas velocity dispersions in a way more directly comparable to IFU measurements in a suite of cosmological zoom disc simulations. While they find that changes in the dispersion are temporally correlated with both gas accretion on to the galaxy discs and the global SFR, they were unable to draw conclusions about the cause of this correlation. On the other hand, Ceverino et al. (2017) examined the driver of σ with z. By running a controlled experiment in which feedback was shut off for a short time, Ceverino et al. (2017) found that gravitational instabilities in a marginally stable disc set a floor to the turbulence scale, but that feedback drives gas dispersions higher than gravitational instabilities alone. Simulations without feedback did not show the declining velocity dispersion with time. They suggest that the decline is tied to the decreasing gas fractions, and hence SFR, of the simulated discs with time.

In this paper, we use a high-resolution cosmological zoom-in simulation to simultaneously investigate the detailed kinematics of the present-day galaxy as well as the galaxy's kinematic evolution

over cosmological time-scales. In fact, this simulation, h277,[2] is one of the simulations studied by Kassin et al. (2014), and thus it has already been shown that this specific galaxy matches the observed trends of decreasing gas velocity dispersion with time. We focus on this particular galaxy as it has many properties similar to the MW, including a relatively quiescent merger history and structural parameters within 10 per cent of the MW at $z = 0$ (Loebman et al. 2014). The simulation tracks molecular hydrogen abundances and cooling processes (Section 2) and thus resolves a multiphase ISM that allows the low $\sigma_{\rm birth}$ of young stars to be captured. In Section 3, we establish that the AVR of h277 at $z = 0$ is nearly a perfect match to the MW (Section 3.1). We investigate how $\sigma_{\rm birth}$ varies with radius and time in Sections 3.2 and 3.3, and show that the same equilibrium model that matches the settling of disc kinematics with z also matches the evolution of $\sigma_{\rm birth}$ in this individual galaxy (Section 3.4). In Section 4, we first discuss the physical processes causing h277 to match the MW's AVR (Section 4.1), and then highlight the numerical aspects of the simulation that have allowed these processes to emerge (Section 4.2). We conclude in Section 5.

2 THE SIMULATION

In this work, we use a cosmologically derived (WMAP3; Spergel et al. 2003) Milky Way–mass galaxy evolved for 13.7 Gyr using the parallel *N*–body+SPH code GASOLINE (Wadsley, Stadel & Quinn 2004). The simulation uses a redshift-dependent cosmic UV background (Haardt & Madau 2001) and realistic cooling and heating, including cooling from metal lines (Shen, Wadsley & Stinson 2010) and H_2 (Christensen et al. 2012). Feedback from supernovae type II (SN II) is modelled using the 'blastwave' approach (Stinson et al. 2006) in which 10^{51} erg of thermal energy is deposited per SN, and cooling is temporarily disabled based on the local gas characteristics. SN Ia thermal energy is also injected, but cooling is not disabled. The probability of star formation is a function of the non-equilibrium H_2 abundances (Christensen et al. 2012). The result of tying the star formation to the molecular hydrogen abundance is a greater concentration of the stellar feedback energy and the more efficient generation of outflows. These outflows ensure that the final galaxy has an appropriate rotation curve (Governato et al. 2012; Christensen et al. 2014), stellar mass fraction (Munshi et al. 2013), metallicity (Christensen et al. 2016), and H I properties (Brooks et al. 2017).

The galaxy we use, h277, is a part of the *g14* suite of simulations (Christensen et al. 2012), and has been studied extensively elsewhere in the literature (e.g. Loebman et al. 2012, 2014), including a demonstration that it has a realistic dwarf satellite population (Zolotov et al. 2012; Brooks & Zolotov 2014). This galaxy has a gravitational force resolution of 173 pc and mass resolutions of $1.3 \times 10^5 \, M_\odot$, $2.7 \times 10^4 \, M_\odot$, and $8.0 \times 10^3 \, M_\odot$ for the dark matter, gas, and stars, respectively. It also includes the large-scale environment by using the 'zoom-in' volume renormalization technique (Katz & White 1993) when creating the initial conditions. The zoom-in volume contains 3072^3 particles and is a cube 50 comoving Mpc per side, ensuring the capture of large-scale tidal torques thought to build a galaxy's angular momentum.

The virialized halo at every step was identified using Amiga's Halo Finder (AHF; Gill, Knebe & Gibson 2004; Knollmann & Knebe

2009). AHF calculates $M_{\rm vir}$ as the total mass within a sphere that encloses an overdensity (following Bryan & Norman 1998) relative to the critical density $\rho_{\rm crit}(z)$. At redshift zero, h277 has a virial radius $R_{\rm vir}$ of 227 kpc and $M_{\rm vir}$ of $6.8 \times 10^{11} \, M_\odot$. Of this, 7 per cent is in gas, 6 per cent is in stars, and 87 per cent is in dark matter. A total of 4.6×10^6 dark matter, 2.1×10^6 gas, and 7.4×10^6 star particles are within the virial radius at redshift zero.

The present-day structure and accretion history of h277 share some similarities with the MW. The simulated galaxy has a relatively quiescent merger history, with the last major merger (3:1 halo mass ratio) occurring at $z \sim 3$. The MW is also known to have a quiet accretion history (e.g. Ruchti et al. 2015). The present-day stellar mass of h277 ($4.1 \times 10^{11} \, M_\odot$) and maximum circular velocity (~ 235 km s^{-1}) are within ~ 10 per cent of those measured in the Milky Way (Bland-Hawthorn & Gerhard 2016). Still, the simulation is not, nor was it designed to be, a perfect match to the MW. The present-day *r*-band bulge to disc ratio is 0.33 (applying GALFIT to SUNRISE-processed images, Peng et al. 2010; Jonsson 2006, respectively).

3 RESULTS: THE PRESENT-DAY AVR

To analyse the present-day AVR of h277, we wish to define a region that is solar neighbourhood-like. Boardman et al. (2020) showed that the scatter in radial gradients of MW analogues is minimized if galaxies are normalized by disc scale length, $R_{\rm d}$. The best-fitting exponential profile to the disc-dominated ($R > 2.5$ kpc) stellar surface mass density yields $R_{\rm d} = 2.42$ kpc. For the Milky Way, Bovy & Rix (2013) find $R_{\rm d} = 2.15$ kpc for the disc mass surface density profile. The ratio of these scale lengths is equivalent to the ratio of the central radius of the simulated solar annulus to the MW Galactocentric solar radius, $R_\odot$. Adopting $R_\odot = 8$ kpc, the simulated solar radius is $R = 9$ kpc and a solar neighbourhood-like annulus spans $8.0 < R/{\rm kpc} < 10.0$. We calculate all velocity dispersions using the robust biweight midvariance estimator as implemented in ASTROPY.[3]

The present-day age-resolved stellar kinematics of h277 reveal a clear AVR in the disc ($|z| < 1$ kpc) at the scaled solar annulus (Fig. 1). The youngest stars are dynamically cold, with a vertical velocity dispersion $\sigma_z \sim 8$ km s^{-1}, which is consistent with the cloud-to-cloud velocity dispersion measured in molecular gas of GMCs in the MW and nearby galactic discs (Stark & Brand 1989; Wilson et al. 2011) and noteworthy for a cosmological zoom-in simulation (see Section 4 for discussion). The velocity dispersion increases with age τ for older stars; σ_z gradually increases to ~ 30 km s^{-1} at $\tau = 10$ Gyr and then quickly rises to ~ 80 km s^{-1} for the oldest stars (black line).

While h277 was not designed to reproduce the MW, the detailed measurements of the MW AVR offer an informative context to interpret our findings. The intrinsic AVR of h277 (black line in Fig. 1) is very similar to the MW AVR, but the oldest stars ($\tau > 9$ Gyr) are significantly hotter than what is observed. However, direct comparison of empirical results with the simulated AVR, where all relevant data are known perfectly and completely, can be misleading. The MW data are from the local solar neighbourhood, volume-complete Geneva Copenhagen Survey (GCS; Nordström

---

[2]We note that a version of h277 was also studied by House et al. (2011). However, the version in this paper has twice the spatial resolution, $8\times$ the mass resolution, and includes an updated ISM and star formation prescription as described in Christensen et al. (2012).

[3]$\sigma(v) = \sqrt{\zeta_{\rm biweight}(v)}$. When drawing from a normal distribution with known parameters, we found the biweight mid-variance to outperform the straightforward moment calculation at small sample size ($N < 20$); the two methods are nearly indistinguishable for larger N (see Beers, Flynn & Gebhardt 1990)
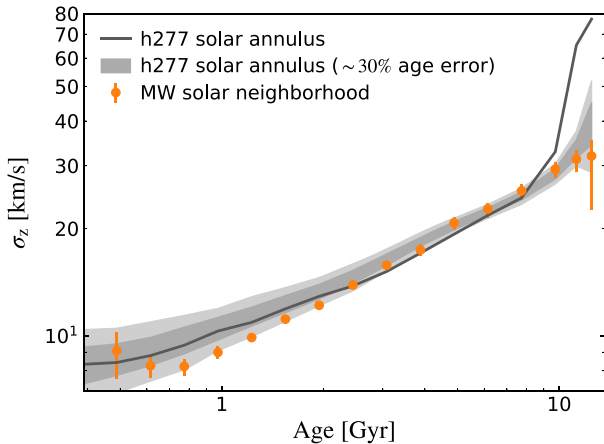
Figure 1. The vertical velocity dispersion as a function of stellar age in the 'solar neighbourhood' of h277 (black line) compared to the analogous AVR measurement in the Milky Way (orange points, data from Casagrande et al. 2011). The dark and light grey bands represent the $16 - 84$ per cent and $5 - 95$ per cent, respectively, range of AVRs that would be found in h277 after accounting for the sample size, age bias, and measurement uncertainty of the re-calibrated GCS survey of the local solar neighbourhood. See the text for details.

Figure 2. The temporal evolution of the vertical velocity dispersion, σ_z, for coeval stellar populations (or mono-age populations, MAPs) found in the present-day solar annulus (coloured lines) and the star-forming gas reservoir (black line). Line colour corresponds to MAP age; darker colours represent increasingly younger stellar populations (see legend). The beginning of each line corresponds to the lookback time and σ_z when a MAP formed. MAPs are born with the kinematics of the gas reservoir at the time of their birth. Both 'Upside-Down' formation and dynamical heating play a significant role in creating the present-day AVR. Older stellar populations are born dynamically hotter than younger ones, and σ_z increases for all MAPs following their birth.

et al. 2004; Holmberg, Nordström & Andersen 2009). Casagrande et al. (2011) performed the latest re-calibration of the GCS stellar parameters using the infrared flux method on a subset of stars with the relative 'best photometry'. We show the MW AVR (orange points) using the $N_{GCS} = 3168$ stars in this *irfm* sample with 'good age' measurements (Casagrande et al. 2011). Even these high-fidelity data are not perfect: they have a known bias towards younger stars (e.g. Nordström et al. 2004; Casagrande et al. 2011), a mean relative age uncertainty of 28 per cent, and are a discrete sampling of the underlying age and kinematic distribution (as $N_{GCS} \ll$ the number of stars within the solar annulus). The simulation data must be 'degraded' with these sources of noise and bias in order to perform a more legitimate comparison of the h277 and MW AVRs (see also Martig et al. 2014; Aumer et al. 2016).

The AVR of h277 is consistent with the MW AVR at all ages after accounting for the measurement noise and bias of the empirical data (grey-shaded regions, Fig. 1). The σ_z measured from mock surveys of the h277 solar annulus peak at just 25 to 40 km s^{-1} for the oldest stars while maintaining < 10 km s^{-1} σ_z at $\tau < 1$ Gyr (grey bands in Fig. 1). Each mock survey contains N_{GCS} stars randomly drawn from the solar annulus mid-plane ($8 < R < 10$ kpc and $|z| < 1$ kpc); we then add 0.12 dex uncertainty in $\log \tau$ (~ 25 per cent relative uncertainty at $\tau = 4$ Gyr) and generate the mock ages. Differences in the AVR measured from the intrinsic (black line) and generated mock data (grey regions) are driven by the intrinsic age distribution and the synthetic noise. The intrinsic AVR is usually not at the median of the median observed AVR. The intrinsic stellar age distribution at the solar annulus mid-plane peaks at $\tau \sim 7.5$ Gyr. The large difference between the black line and grey regions for $\tau > 10$ Gyr is due to the fact that age errors strongly skew the distribution towards younger, and therefore dynamically colder stars. In a similar fashion, at $\tau = 4$ Gyr the errors introduce a bias towards older stars, causing the grey band of possible observed AVRs to fall above the intrinsic AVR.

As far as we can ascertain from the literature, h277 is the only cosmological zoom-in simulation with a present-day AVR consistent with the MW at the level found here across 13 Gyr of evolution.
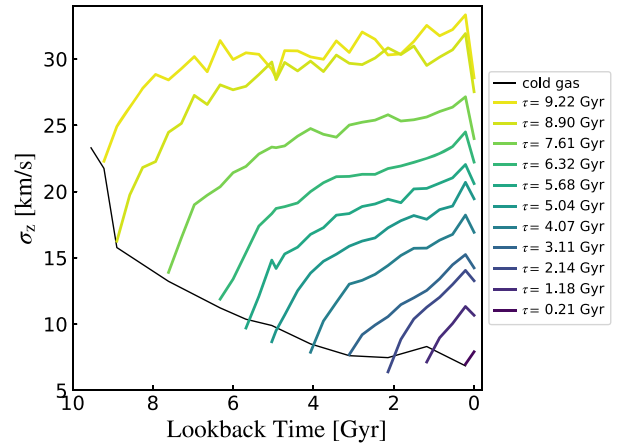
3.1 The origin of the AVR

We now investigate how the present-day AVR came to be. Fig. 2 shows the temporal evolution of σ_z for several stellar cohorts that end the simulation in the solar annulus. These cohorts are mono-age populations (MAPs); they contain stars born within a narrow range of formation time ($\Delta t_{form} = 50$ Myr).[4] With this Δt_{form} resolution, the median (minimum) number of star particles in a given MAP is 1131 (346) for the populations shown in Fig. 2. The end points of each evolutionary track represent the present-day kinematics of each MAP, as encapsulated by the AVR discussed above. In slight contrast to Fig. 1, we use all stars in the solar annulus, regardless of vertical position, as height restrictions would introduce phase correlations that can create a biased view of the velocity dispersion histories (Aumer et al. 2016). We track the kinematic evolution of both the stellar MAPs (colour-coded lines) and the cold (<1000 K) gas (thin black line) as function of lookback time ($t_{lookback}$).

The kinematics of the star-forming gas reservoir regulate the assembly of the disc. At each formation epoch, we calculate the σ_z of the star-forming gas reservoir using the cold gas ($T < 1000$ K) that is spatially coincident with the MAP at birth; i.e. is within the annulus defined by the inner quartile range of formation radius of each MAP. The *in-situ* σ_z of MAPs at birth are nearly equal to that of the cold gas. Stars clearly inherit the kinematics of the gas from which they form. The star-forming gas reservoir collapses and becomes dynamically colder over time; σ_z decreases from ~ 20 km s^{-1} nearly 10 Gyr ago to 7 km s^{-1} in the present-day. In turn, progressively younger MAPs form with decreasing σ_z. Bird et al. (2013) called this behaviour 'Upside-Down' formation. It has been recognized in a wide range of recent cosmological zoom-in simulations (e.g. Grand et al. 2016; Ma et al. 2017), but its role in disc kinematics over

---

[4] We confirm that the measured σ_{birth} does not change for smaller values of Δt_{form}, see Section 4.2.3
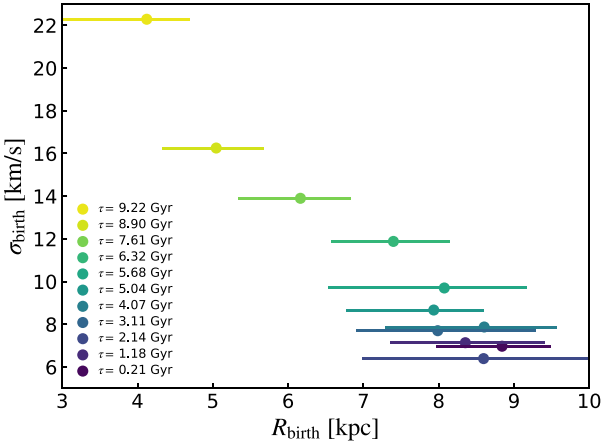
Figure 3. The relationship between vertical kinematics at birth and formation radius of MAPs found in the present-day solar annulus. Points represent a MAP median formation radius and the velocity dispersion at birth; error-bars indicate the interquartile range of R_{birth}. MAPs with earlier formation times (colour-coding is identical to Fig. 2) were generally born at smaller formation radii and larger σ_{birth} than their younger counterparts.

the last 10 Gyr is still debated (see Section 4). Fig. 2 qualitatively resembles fig. 19 of Bird et al. (2013), but in this simulation the birth values of σ_z are lower, especially at late times, and growth of σ_z by heating plays a larger role (see section 4.2.3). The star-forming gas σ_z decreases in an exponential fashion, dropping by a factor of 2 from $t_{lookback} \sim 10$ Gyr to 6 Gyr but remains nearly constant (~ 7 km s^{-1}) for $t_{lookback} < 4$ Gyr. Upside-Down formation establishes a correlation between the formation time of a stellar population and its σ_z at birth due to the evolving kinematics of star-forming gas reservoir.

Stellar populations experience dynamical heating after birth; i.e. the present-day velocity dispersion is greater than σ_{birth} for each MAP (Fig. 2). The heating rate $d\sigma_z/dt$ generally appears velocity-dependent; for each MAP, it is highest just after formation and decreases with increasing σ_z. Gravitational scattering of the stars due to encounters with a perturbing population, such as mid-plane concentrated molecular clouds, would produce the general kinematic evolution seen here (Spitzer & Schwarzschild 1951; Lacey 1984). Indeed, the shape of the $\sigma_z(t_{lookback})$ tracks are qualitatively similar to those of MAPs in idealized dynamical heating experiments (e.g. Aumer et al. 2016). We will investigate the details of the dynamical heating mechanism(s) in future work. Ultimately, it is clear that h277's present-day kinematics result from the detailed balance of the collapsing star-forming gas reservoir and the dynamical heating experienced by MAPs after birth.

3.2 Formation radius and σ_{birth}

Many of the stars currently at the solar cylinder were not born there. Fig. 3 shows that older stellar populations that end the simulation in the solar annulus were born at smaller radii, R_{birth}, compared to their younger counterparts. The figure shows the velocity dispersion of the MAP at birth, σ_{birth}, as a function of R_{birth}. There is a clear trend for stars in the present-day solar neighbourhood: progressively younger MAPs were born at larger R_{birth} and smaller σ_{birth}.

This is expected for two reasons. First, the trend in age versus birth radius seen in Fig. 3 is a clear sign of inside-out disc growth

in h277. The older stars formed in a more centrally concentrated disc. Very few 10 Gyr old stars were born in the solar annulus. The vast majority were born in the interior of the disc but are found in the solar annulus at $z = 0$. Secondly, the decreasing trend in σ_{birth} with decreasing age is indicative of disc settling. The oldest stars considered here have a small median formation radius and large birth velocity dispersion $(R_{birth}, \sigma_{birth}) = (\sim 4$ kpc, 22 km s$^{-1})$. At the other extreme, the youngest stars born in the solar annulus have the largest formation radii and are amongst the dynamically coldest at birth $(R_{birth}, \sigma_{birth}) = (\sim 9$ kpc, 7 km s$^{-1})$.

Fig. 3 shows that birth radius and birth kinematics are correlated. Stars born at smaller (larger) galactocentric radii are kinematically hotter (colder) at birth. The exponential scale length (R_d) of the stellar disc gradually increases from ~ 1.2 kpc to 2.5 kpc during the past 10 Gyr due to the inside-out growth of the disc. Over that same time period, R_d of the newly formed stars ($\tau < 50$ Myr) increases from ~ 1.5 kpc to 4.5 kpc and is always greater than the scale length of the entire stellar disc at any epoch. This inside-out growth is directly coupled to the disc cooling seen in Upside-Down evolution. Since age and formation radius are correlated, birth velocity dispersion is also strongly correlated with formation radius as the galaxy's disc cools; i.e. as the galaxy grew outwards, it also grew kinematically cooler. Thus, the σ_{birth} of an MAP can be a function of both R_{birth} as well as age.

3.3 SFR density and σ_{birth}

In the bottom panel of Fig. 4, we show how σ_{birth} varies as both a function of formation position and epoch in the disc. Several patterns emerge. First, the typical σ_{birth} in the disc increases with lookback time; i.e. 'Upside-Down' formation occurs across the entire disc. Secondly, σ_{birth} has a negative large-scale radial gradient over the last ~ 10 Gyr; i.e. the outer disc is dynamically colder than the inner disc at all times. Thus, the same trends that were seen for solar annulus MAPs also hold for the entire disc.

Fig. 4 (bottom panel) also shows that the most dramatic evolution of σ_{birth} occurs when combining both the temporal and radial gradients, moving from the upper left to the bottom right-hand of the panels. The greatest discrepancy in σ_{birth} is found when comparing older stellar populations born in the inner disc with young stars that formed in the outer disc. These trends manifest themselves in the AVR of the solar neighbourhood.

To make these radial profiles, we divide the disc into a grid in (R, θ). Radial annuli are spaced 0.5 kpc apart and further divided into 18 azimuthal bins ($\Delta\theta = 20°$). The velocity dispersion profiles shown here are azimuthally averaged within each annulus. In general, these results are consistent with what one would find by binning in radius only. In the outer disc, however, warps from either satellite encounters (generally not applicable for h277 over the last 10 Gyr; Section 2) or gas accretion (Roškar et al. 2010) can change the mean velocity of gas and stars on one side of the galaxy versus the other, which would artificially increase the measured dispersion if the annulus was taken as a whole. Furthermore, the Toomre stability criterion and many forms of potential pressure support to the ISM act locally; if the gas is not well-mixed within an annulus or experiences a much different gravitational potential (more likely in the outer galaxy due to the significantly longer dynamical time), then the velocity dispersion should be calculated on more local scales.

The top panel of Fig. 4 shows that the surface density of star formation, $\dot{\Sigma}_\star$, varies with radius and lookback time in the same qualitative fashion as σ_{birth}. At a specific lookback time, the inner disc has higher $\dot{\Sigma}_\star$ than the outer disc, and $\dot{\Sigma}_\star$ generally decreases
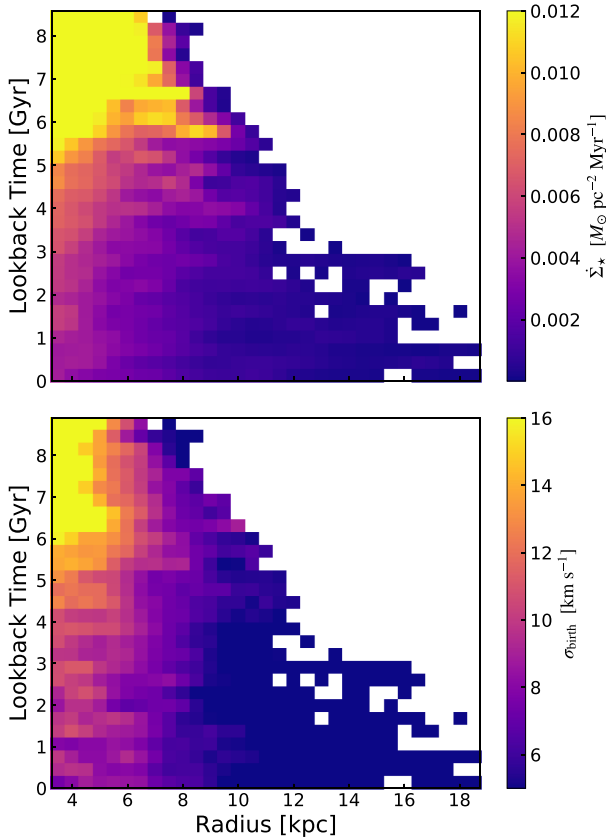
Figure 4. The star formation rate surface density (top) and the velocity dispersion of stars at birth (bottom) as a function of radius and time. We independently smooth each radial profile to emphasize trends; pixel colour corresponds to the running mean value across 1.5 kpc in radius (3 pixels). At a given epoch (row), $\dot{\Sigma}_\star$ is typically highest in the inner galaxy and gradually decreases as the galactocentric radius increases. At a fixed radius (column), $\dot{\Sigma}_\star$ is generally highest at early times and decreases towards the present-day. The radial and temporal gradients in $\sigma_{\rm birth}$ are very similar. Both $\sigma_{\rm birth}$ and $\dot{\Sigma}_\star$ are strongly correlated at the local spatial scale over much of the galaxy's history.

towards the present-day. We find that the relationship between $\dot{\Sigma}_\star(R, t_{\rm lookback})$ and $\sigma_{\rm birth}(R, t_{\rm lookback})$ is strongly correlated; this is visible in the nearly one-to-one colour correspondence between $\dot{\Sigma}_\star$ and $\sigma_{\rm birth}$. While the dynamic range of each panel image is different, the colour scale of each panel is linear, and the different dynamic ranges of each panel are suggestive of the slope of the relationship. Strong correlation between a gaseous component velocity dispersion and $\dot{\Sigma}_\star$ is expected on theoretical grounds when combining the Toomre stability criterion and the Kennicut-Schmidt law (discussed further below) and has been observed in star-forming galaxies (e.g. Yu et al. 2019; Sun et al. 2020). We find that $\dot{\Sigma}_\star$ correlates with $\sigma_{\rm birth}$ at the site of star formation and that this correlation exists throughout the disc and for at least the past ~ 10 Gyr of evolution.

3.4 Disc stability

We characterize the evolution of $\sigma_{\rm birth}$ for the global disc in Fig. 5. Here, we define the radius of the star forming disc, $R_{\rm disc}$, to be the radius that encloses 80 per cent of the ongoing star formation. We measure $\sigma_{\rm birth}$ in an annulus at $R_{\rm disc} \pm 0.5$ kpc. The upside-down formation of the disc is clearly seen as $\sigma_{\rm birth}$ decreases towards the
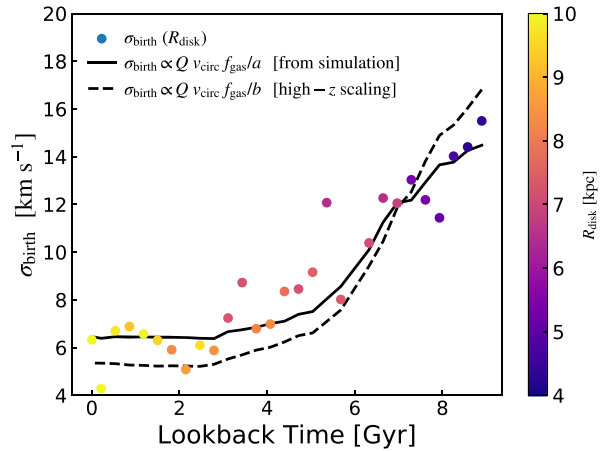

Figure 5. Comparison of simulation measurements and gravitational equilibrium-driven predictions for the evolution of $\sigma_{\rm birth}$. Points show the vertical velocity dispersion of newly formed stars in an annulus at $R_{\rm disc}$ as a function of $t_{\rm lookback}$, coloured by $R_{\rm disc}$. $R_{\rm disc}$ is the radius that encloses 80 per cent of ongoing star formation, and $\sigma_{\rm birth}$ is measured within an annulus at $R_{\rm disc} \pm 0.5$ kpc. $R_{\rm disc}$ increases towards the present-day as the disc grows inside-out. The two black lines are predictions for the evolution of $\sigma_{\rm birth}$ assuming the disc is marginally stable. See the text for details. Both models predict a disc settling process very similar to what is measured, suggesting that the disc is continuously driven towards marginal gravitational instability, which plays a strong role in governing the slow collapse of the star-forming gas reservoir (and hence $\sigma_{\rm birth}$).

present day (coloured points). The velocity dispersion of stars at birth decreases by a factor of ~ 2.5 over the last 10 Gyr, but much of that evolution occurred early and $\sigma_{\rm birth}(R_{\rm disc})$ remains below 8 km s^{-1} over the past 5 Gyr. The disc also grows outwards during this time; $R_{\rm disc}$ steadily increases as star-formation proceeds further out in the disc (represented by the colourbar in Fig. 5; see also Minchev, Chiappini & Martig 2013). Empirically, as h277 grows inside-out, it also grows upside-down.

The kinematic evolution of $\sigma_{\rm birth}$ is in good agreement with scaling arguments under the assumption that the disc is in equilibrium, i.e. that the disc remains quasi-stable as new gas accretes on to the galaxy to replace gas lost to star formation and outflows (e.g. Thompson, Quataert & Murray 2005; Davé, Finlator & Oppenheimer 2012; Krumholz, Dekel & McKee 2012; Dekel & Mandelker 2014). If the gas component provides the dominant component to the mid-plane pressure, the Toomre relation (Toomre 1964) of the star-forming gas reservoir can be rewritten as

$$\sigma_{\rm birth}/v_{\rm circ} = \psi f_{\rm gas} Q/\sqrt{2}, \tag{1}$$

where $v_{\rm circ}$ is the rotation speed, Q is the Toomre parameter, ψ is a constant of order unity, and $f_{\rm gas}$ is the gas fraction (Genzel et al. 2011). The $\sqrt{2}$ factor stems from the epicyclic frequency component of the Toomre relation and our assumption of a flat, or nearly flat, rotation curve. The quantity $f_{\rm gas}$ is the fraction of the overall mass in gas that contributes to the effective gravitational potential felt by the newly forming stars.

We next demonstrate that $\sigma_{\rm birth}(R_{\rm disc})$ can be reproduced assuming a Toomre stable disc, with $\sigma_{\rm birth}$ being determined by the evolving gas fraction $f_{\rm gas}$. The circular velocity at $R_{\rm disc}$ is nearly constant, varying less than ~ 10 per cent, over the past 10 Gyr. The lines in Fig. 5 are model predictions that assume a constant $Q_{\rm gas} = 1$ at $R_{\rm disc}$ for all epochs. We compute $f_{\rm gas}$ in two ways. In the first model, $f_{\rm gas}$

is calculated using the empirical scaling (Tacconi et al. 2013)

$$f_{\text{gas}} = \frac{1}{1 + (\tau_{\text{depl}} \, \text{sSFR})^{-1}}, \qquad (2)$$

where the specific star formation rate sSFR$= \dot{M}_\star/M_\star$ and $\dot{M}_\star$ is measured directly from the simulation as the average SFR over the last 50 Myr and the gas depletion time is modelled as $\tau_{\text{depl}} = 1.5 \times (1 + z)^\alpha$ Gyr with $\alpha = -1.0$.[5] Many empirical studies of resolved spectroscopy of disc galaxies use equation (2) (e.g. Wisnioski et al. 2015). Secondly, we compute the fraction of the gravitational potential due to the gas surface density,

$$f_{\text{gas}} = \left.\frac{\Sigma_{\text{gas}}}{\Sigma_{\text{tot}}}\right|_{R_{\text{disc}}}, \qquad (3)$$

where $\Sigma_{\text{tot}}(R) = v_{\text{circ}}^2/(\pi G R)$ is the total dynamical surface density. The gas surface density is not for all gas, just the fraction of the ISM that contributes to the vertical mid-plane pressure felt by the newly forming stars (e.g. Thompson et al. 2005; Krumholz et al. 2012). To best track the mass of the ISM directly contributing to star formation, we select all gas with a density higher than 1 atoms cm^{-3}. Here, f_{gas} is evaluated at R_{disc}.

We can rewrite equation (1) as $\sigma_{\text{birth}} \propto v_{\text{circ}} f_{\text{gas}} Q/C$, where C is a constant chosen to match the normalization of $\sigma_{\text{birth}}(t)$. Fig. 5 shows C $= 2$ when f_{gas} is set by the empirical high-z scaling (dashed line), and C $= 0.4$ when f_{gas} is set by the dense gas surface density in the simulation (solid line). The evolving gas fraction largely determines the shape of both lines as v_{circ} changes by only ~ 10 per cent, and the Toomre Q parameter is assumed constant ($Q = 1$).

Note that the recast marginal stability argument is not a fit to the σ_{birth} measurements, yet it predicts a disc settling process very similar to what is measured. This suggests that the disc is continuously driven towards marginal gravitational instability, which plays a strong role in governing the slow collapse of the star-forming gas reservoir (and hence σ_{birth}).

4 DISCUSSION

In this section, we first discuss the key physical processes that occur in the simulated galaxy that result in the excellent match to the Milky Way's AVR at $z = 0$. We then compare to previous simulation work, and highlight the key numerical achievements that have allowed these physical processes to occur.

4.1 Matching the Milky Way's AVR

We find (Fig. 1) that the solar neighbourhood AVR measured in h277 is nearly identical to the AVR in the solar neighbourhood of the MW. This is true for stellar populations that span more than 10 Gyr in age. The primary physical process that allows h277 to match the AVR over such a large age range is disc settling, or upside-down formation, combined with inside-out disc growth. We discuss below that the resulting $\sigma_{\text{birth}}(z)$ is set by the fact that the stars in the disc are born in equilibrium. Fig. 2 also shows that stellar populations are subsequently heated after birth, and that the velocity dispersion of the cold gas in h277 over the last few Gyr prior to $z = 0$ is an excellent match to the observed σ in star forming gas near the Sun. Below, we discuss these factors that set the AVR.

4.1.1 Stars are born in equilibrium

We have shown that h277 exhibits both inside-out and upside-down formation of disc stars. The inside-out growth of galaxy discs is expected due to the fact that the angular momentum of accreted gas increases with decreasing z (e.g. White & Rees 1978; Fall & Efstathiou 1980). Inside-out growth has been observationally confirmed in relatively massive disc galaxies (e.g. Williams et al. 2009; Gogarten et al. 2010; Barnes et al. 2014; Frankel et al. 2019; Peterken et al. 2020). The theoretical explanation behind the upside-down formation of discs has only more recently been explored, motivated by the observations of kinematically hot discs at high z. It has been shown that this evolution can be modelled if the velocity dispersion of gas evolves according to the gas fraction within a marginally stable disc (e.g. Wisnioski et al. 2015).

We find (Section 3.3) that the velocity dispersion of newly forming stars, σ_{birth}, at any radial position in the disc correlates with the star formation rate surface density, $\dot{\Sigma}_\star$, at that radius over the past 10 Gyr (see Fig. 4). This behaviour is expected if a disc is marginally stable, in dynamical equilibrium, and follows a Schmidt–Kennicutt relation (Schmidt 1959; Kennicutt 1998) for star formation (e.g. Krumholz et al. 2012; Swinbank et al. 2012). Multiwavelength observations of nearby star-forming galaxies confirm a strong correlation between $\dot{\Sigma}_\star$ and the pressure required to stay in dynamical equilibrium (Sun et al. 2020). The star formation prescription adopted for this simulation ensures it follows a Schmidt–Kennicutt relation (Christensen et al. 2012, 2014). It is also clear from Fig. 2 that σ_{birth} tracks the velocity dispersion of the star forming gas, σ_{coldgas}, and σ_{coldgas} should track the neutral gas velocity dispersion σ_{g} to within a factor of two. If the disc has a constant Q_{gas}, $\sigma_{\text{g}} \propto \Sigma_{\text{g}}$, where Σ_{g} is the surface density of the neutral gas. Meanwhile, the Schmidt–Kennicutt relation requires $\dot{\Sigma}_\star \propto \Sigma_{\text{g}}^{1.5}$ (Leroy et al. 2008).[6] Putting it all together, $\sigma_{\text{birth}} \propto \sigma_{\text{g}} \propto \Sigma_{\text{g}} \propto \dot{\Sigma}_\star^{0.67}$ for a stable disc in equilibrium. Using the data from Fig. 4, we find $\sigma_{\text{birth}} \propto \dot{\Sigma}_\star^{\sim 0.4}$. These results suggest that σ_{birth} is governed by something more than a constant Q_{gas}.

On the other hand, Fig. 5 demonstrates that a dynamical equilibrium model can reproduce the trends seen in h277's stellar populations at R_{disc}. For a moderately stable gas disc in equilibrium, the evolution shown in Fig. 5 is driven by the decline in gas fraction, f_{gas}, with decreasing z. Likewise, the evolution of the galactic SFR in h277 nearly matches the qualitative evolution in $\sigma_{\text{birth}}(R_{\text{disc}})$ seen in Fig. 5. The SFR of h277 was a factor of ~ 4–5 higher ~ 10 Gyr ago relative to the current SFR (~ 1 M$_\odot$ yr^{-1}), decreased relatively quickly to 1.5 M$_\odot$ yr^{-1} nearly 5 Gyr ago, and showed little change over the past 4 Gyr. Because we expect that the SFR is tied to the abundance of fuel for star formation, i.e. f_{gas}, it is not surprising that the SFR follows a similar trend. The star formation history of h277 over the last 10 Gyr appears to be fairly consistent with star formation history (SFH) of the Milky Way (e.g. Snaith et al. 2015), which is likely another reason that the AVR of h277 is a good match to the Milky Way's AVR.

What component(s) of the disc are marginally stable? The results in Figs 4 and 5 appear to be in tension at first glance. If $\sigma_{\text{birth}} \propto \dot{\Sigma}_\star^{\sim 0.4}$ from Fig. 4, it suggests that Q_{gas} is not constant, and yet a constant $Q_{\text{gas}} = 1$ appears to match the evolution in Fig. 5. A resolution can be had if the multicomponent Q_{tot} (e.g. Romeo & Wiegert 2011), accounting for contributions from both the gas and stars, is instead the

---

[5]α has been measured between -0.7 and -1.5 (Davé et al. 2012; Tacconi et al. 2013)

[6]There is substantial scatter in the Schmidt–Kennicutt relation at small scales (Christensen et al. 2012; Orr et al. 2019)

conserved quantity and if $Q_{gas} \propto Q_{tot}$ at R_{disc}.[7] Cursory investigation suggests that $Q_{tot}(R, \tau)$ is the quantity that is relatively conserved rather than Q_{gas} across the disc and that the gas and stellar components contribute approximately equally to local stability at R_{disc}. We will investigate the multicomponent stability of the disc in detail in future work. Resolved studies of local star-forming disc galaxies (Romeo & Falstad 2013) and their simulated counterparts (Orr et al. 2019) also connect the kinematics of star-forming gas with multicomponent stability. Conservatively, we conclude a quasi-constant Q_{tot} is plausible and consistent with all of the results in this paper.

Vertical hydrostatic equilibrium is a common assumption in analysis of the ISM, and controlled, high-resolution simulations show that equilibrium is quickly established even with a wide range of initial conditions (e.g. Koyama & Ostriker 2009; Kim, Ostriker & Kim 2013). Controlled simulation experiments have shown that galaxies naturally regulate their star formation, striking a balance between the pressure support in the mid-plane and the weight of the ISM, even when varying sub-grid physics (e.g. Benincasa et al. 2016). In future work, we will determine the local gravitational stability of the disc and test the reasonable assumption that stars are born from gas in hydrostatic equilibrium with the local disc.

4.1.2 Heating/radial mixing

The formation radius of the stars has a big role to play in σ_{birth}, not just the time at which they formed. This is because the galaxy is not only forming upside-down, but inside-out. The effective radius of the disc (R_{disc}, the mass or light-weighted mean radius of newly formed stars) moves outwards as the galaxy grows (Fig. 5). As we have just established, older stars are born at a time when σ_{birth} is higher, likely due to the higher f_{gas} of the disc while in marginally stable equilibrium, and a higher SFR. For h277, the oldest stars contributing to the AVR were also born at roughly half of the radius of the solar neighbourhood. Younger stars are born with lower σ_{birth}, and closer to the solar annulus.

As can be seen in Fig. 4, even at $z = 0$ the inner disc has a higher σ_{birth}. Therefore, both a smaller formation radius and older age contribute to higher σ_{birth}. As can be read from the bottom panel of Fig. 4 (upper left to lower right), this evolution leads to a maximizing of the evolution of σ_{birth} for stars that end up in the solar neighbourhood at $z = 0$. The radial dependence of σ_{birth} increases the difficulty of inferring the *in-situ* birth kinematics of a stellar population given present-day observations. The dynamic range and distribution of σ_{birth} for stars at any present-day radius is influenced by both $\sigma_{birth}(\tau)$ and the history of stellar radial mixing away from R_{birth} specific to the galaxy of interest. How the stars migrated away from their birth radii, whether by changes in orbital angular momentum (e.g. Sellwood & Binney 2002) or simple increases in orbital energy due to gravitational scattering, does not alter this conclusion.

It is clear from Fig. 2 that stellar populations in the solar neighbourhood at $z = 0$ have been heated after birth. *In-situ* kinematics at birth account for nearly half of the present-day velocity dispersion of each solar neighbourhood MAP ($\sigma_{birth}/\sigma_z \sim 0.4$; Fig. 2).[8] The source of the heating is likely responsible for the radial mixing as well. Although mergers have been shown to heat the disc (Martig et al. 2014; Grand et al. 2016; Buck et al. 2020), h277 has a very quiescent merger history over the past 10 Gyr, so mergers are unlikely

to be a major source of heating in this particular galaxy. We note that Grand et al. (2016) found that a central bar is one of the strongest factors in radial mixing, and h277 had a bar in its past. Also, as we discuss further below, h277 is capable of resolving the cold, clumpy structure of the ISM. It has long been suggested that scattering of stars off molecular clouds could heat a stellar population as it ages (Spitzer & Schwarzschild 1951). The fact that the heating rate of the MAPs depends on velocity (Fig. 2) strongly suggests that GMC scattering is occurring in h277.

Leaman et al. (2017) used a dwarf galaxy simulation with identical physics to h277 to investigate the AVR in the Wolf–Lundmark–Melotte (WLM) galaxy. They assumed that σ_{birth} was tied to the SFH (and hence f_{gas}) of WLM, again adopting an equilibrium model. They showed that additional GMC heating after birth could fully explain the stellar dynamics of the simulated dwarf, which was an excellent match to the AVR of WLM. However, they concluded that σ_{birth} plus GMC heating alone is insufficient to explain the AVR in more massive disc galaxies like the MW, and that additional heating by mergers or bars is necessary. However, Leaman et al. (2017) did not consider the impact of R_{birth} on σ_{birth}. Our results suggest that the σ_{birth} of old stars in the present-day solar neighbourhood is likely enhanced over the global $\sigma_{birth}(\tau)$ prediction due to their small R_{birth}. If so, additional heating from mergers would be unnecessary for stars younger than ~ 10 Gyr. In contrast, there have been recent claims that the detailed AVR of the MW (for $\tau \lesssim 8$ Gyr) can arise solely from steady dynamical heating from giant molecular clouds and, optionally, spiral waves, without the need for an evolving σ_{birth} (Ting, Hawkins & Rix 2018; Mackereth et al. 2019).

We note that it is nearly impossible, based only on the present-day vertical kinematics of these stars, to distinguish between a pure dynamical heating evolutionary history and disc settling combined with heating. The evolution of vertical energy ($E_z \sim \sigma_z^2$) due to gravitational orbit scattering is $dE_z/dt \sim \Sigma_{pert}/E_z$, where Σ_{pert} is the surface density of the orbit perturbers (Binney & Tremaine 2008). The E_z dependence of the heating rate means that there is little difference, at a fixed Σ_{pert} (typically the surface density of molecular clouds), in the present-day vertical energy of, e.g. a ~ 7 Gyr population with $\sigma_{birth} = 15$ km s^{-1} versus 7 km s^{-1}. This is because any increase in σ_{birth} is largely negated by a decreased heating rate. However, there is hope to distinguish between these evolutionary tracks using the shape of the velocity ellipsoid, σ_z/σ_r, (see e.g. Mackereth et al. 2019), which is more sensitive to the particular heating history (e.g. Lacey 1984; Jenkins & Binney 1990; Ida, Kokubo & Makino 1993; Sellwood 2008). We will examine the connection between the velocity ellipsoid and the kinematic history of h277's solar neighbourhood stars in a future work.

4.2 Comparison to previous work

As we have just discussed, it is the fact that σ_{birth} decreases with decreasing redshift, combined with the fact that the disc is growing inside-out, that is the primary origin of the solar neighbourhood AVR in h277. Subsequent heating also plays a role. Below we compare our results from h277 to previous simulation results, and establish that it is the simulation's ability to produce dynamically cold gas that allows both the upside-down and inside-out growth to emerge.

4.2.1 Dynamically cold gas

To the best of our knowledge, this simulation is the first cosmological zoom-in MW-mass simulation to recover the low velocity dispersions

---

[7]The relationship between Q_{gas} and Q_{tot} need not be linear away from R_{disc}.
[8]In fact, there is a small range in $\sigma_{birth}/\sigma_z \sim [0.4, 0.5]$, with the oldest stars having the lowest ratio and younger stars having the highest ratio

of young stars in the solar neighbourhood at $z = 0$. In h277, stars forming in the solar neighbourhood over the last 3–4 Gyr before $z = 0$ are born with exceptionally cold dynamics, with a velocity dispersion as low as $\sim$6 km s^{-1}. This velocity dispersion is consistent with the internal kinematics of nearby molecular clouds in the MW (Stark & Brand 1989) and the average cloud-to-cloud velocity dispersion of molecular gas in nearby disc galaxies (6.1 $\pm$ 1.0 km s^{-1}; Wilson et al. 2011). The ability to form stars with this low dispersion is critical to matching the MW AVR, particularly for young stars.

h277 adopts the star formation recipe from Christensen et al. (2012), which explicitly follows the non-equilibrium formation and destruction of H$_2$, and restricts star formation to occurring only in the presence of H$_2$. This restriction ensures that stars are born from a much dynamically colder star-forming gas reservoir, with low temperatures and at high densities ($T < 1000$ K, $n > 100$ atoms cm^{-3}).

The non-equilibrium H$_2$ recipe adopted here seems to be the key to setting a low $\sigma_{\rm birth}$ at the present day. House et al. (2011) examine how $\sigma_{\rm birth}$ varies with star formation prescription, and find that a dispersion 'floor' is created if cold gas is not resolved (see also Martig et al. 2014). Likewise, Kumamoto et al. (2017) show that as the threshold for star formation is decreased, $\sigma_{\rm birth}$ increases because the star forming region becomes 'thicker.'

At higher star formation thresholds, and thus higher $\sigma_{\rm birth}$, upside-down disc settling cannot occur because the disc is born hot. This is seen in earlier works (House et al. 2011; Martig et al. 2014) in which quiescent discs are born with a constant (high) $\sigma_{\rm birth}$ over the last 9–10 Gyr instead of cooling with time. Likewise, if the cold, clumpy ISM isn't resolved, then subsequent heating due to GMC scattering is weakened. Even if GMC scattering is present, the heating rate is diminished if the stellar population is already born hotter, as discussed above. Thus, it is the ability of h277 to capture this dynamically cold gas that allows the primary processes that set the AVR to emerge.

Kumamoto et al. (2017) studied the evolution of $\sigma_{\rm birth}$ in isolated, non-cosmological disc galaxies, and found results very similar to those in h277. With their high resolution, they were able to form stars at similar densities as in h277 ($n > 100$ atoms cm^{-3}), but even colder temperatures ($T < 100$ K). The stars in their simulation have $\sigma_{\rm birth}$ as low as 3 km s^{-1}. As in h277, Kumamoto et al. (2017) find that $\sigma_{\rm birth}$ decreases in their simulated galaxy as $f_{\rm gas}$ decreases. Because they are able to resolve the clumpy ISM, they also find that stellar populations were heated after birth due to GMC scattering, and that the rate of heating decreases with time as the amount of dense gas decreases.

h277 appears to be the first cosmologically simulated disc galaxy to reproduce the low σ values observed in GMCs, allowing it to match the observed AVR in the MW's solar neighbourhood. The results of Kumamoto et al. (2017) may suggest that $\sigma_{\rm birth}$ could be even lower if lower temperatures could be used for star forming gas. On the other hand, observationally $\sigma_{\rm birth}$ seems to be $\sim$6 km s^{-1} (e.g. Stark & Brand 1989; Wilson et al. 2011) rather than the 3 km s^{-1} found in Kumamoto et al. (2017), so it is possible that something acts to keep the dispersion 'floor' closer to 6 km s^{-1} in real galaxies.

4.2.2 The role of feedback

h277 is not the first cosmological disc galaxy simulation to form stars at high densities and low temperatures, yet it seems to be the first with such a low $\sigma_{\rm birth}$. For example, Sanderson et al. (2020)

show the AVR of simulated MW-mass disc galaxies from the FIRE-2 suite, which forms star particles in self-gravitating molecular gas that can self-shield, at $n > 1000$ atoms cm^{-3}. Despite this high star formation threshold, the youngest stars in their simulations have a (total) velocity dispersion at least 20 km s^{-1} higher than young stars in the MW. This suggests that some other factor may influence $\sigma_{\rm birth}$ in simulations, but that this factor is not as dominant in h277.

Both observationally and theoretically, it has been suggested that there is some threshold $\dot{\Sigma}_\star$ above which supernovae are the dominant driver of turbulence (e.g. Agertz et al. 2009; Tamburro et al. 2009; Stilp et al. 2013). Stellar feedback and supernovae are implemented very differently in FIRE-2 than in h277. h277 adopts the 'blast-wave' SN feedback recipe of Stinson et al. (2006). This model injects only thermal energy from supernovae into neighbouring gas particles, and disables cooling in gas particles that are affected by SN II energy (SN Ia are allowed to immediately cool). The disabled cooling is designed to mimic the adiabatic expansion phase of a supernova remnant, which is not otherwise resolved by the simulation. In contrast, FIRE-2 does not disable cooling, but implements a host of young star feedback which is not accounted for in h277, e.g. photoionization by young massive stars, momentum injection from stellar winds, and radiation pressure on dust (Hopkins et al. 2018).

El-Badry et al. (2016) found that stars in FIRE are able to form in gas that is outflowing due to feedback, which is likely to impart a large $\sigma_{\rm birth}$. We do not see this same effect in our simulations. Rather, the low velocity dispersion of the star-forming gas establishes a pressure 'floor,' and new stars are born with similarly low σ. The numerical implementation and subgrid physics of h277 do not artificially force the star-forming gas to broader velocity distributions.

Given the computational cost of running this galaxy, we have not explored the direct impact of our chosen physics by re-simulating the galaxy with different feedback. However, we can speculate on how the feedback impacts the results given previous work. Agertz et al. (2013) explored the impact of varying feedback models on the ISM in galaxies. They found that the model with delayed cooling, similar to our blastwave model, can better reproduce the star formation history of a galaxy relative to a model with more physically motivated feedback. While it tends to create more hot gas than other models, in the outer disc it predicts a similar gas velocity dispersion. Thus, it is not immediately clear that our velocity dispersion results would be different with a different choice of feedback model. On the other hand, the results from FIRE-2 suggest that the choice of feedback model can definitely play a role in $\sigma_{\rm birth}$.

While feedback in h277 may be injecting turbulent energy that affects the gas dispersion, it appears that it is not substantially boosting $\sigma_{\rm birth}$. The low SFR over the last few Gyr prior to $z = 0$ may help to set the dispersion at a constant, low level. We will explore the role of feedback further in future work. Overall, an equilibrium disc model combined with dynamically cold star formation seems to be the key to setting the AVR normalization in this simulation.

4.2.3 Other factors that impact heating results

The degree to which heating plays a role in shaping the present-day AVR differs slightly from the results of Bird et al. (2013). There, the birth velocity dispersion always accounted for more than half of the present-day value for each MAP, $\sigma_{\rm birth}/\sigma_z \sim [0.6, 0.7]$, with older stars having a higher ratio than younger stars (see their fig. 19). As discussed above, their different star formation threshold

($T < 3 \times 10^4$ K, $n > 5$ atoms cm^{-3}) plays some role, but we have identified additional reasons why our results differ.

Bird et al. (2013) examined a broader swath of the disc ($4 < R < 8$ kpc). As we have seen in this work, extending the inner regions to encompass the inner disc will include hotter stellar populations. Here, rather than adopt a fix radius to define the solar neighbourhood, we have scaled the solar neighbourhood based on the relative difference in scale length R_d of the simulated disc compared to the MW. Boardman et al. (2020) showed that the scatter in various radial properties of disc galaxies is minimized when scaling by R_d, suggesting that this scaling is the best way to directly compare to the MW's AVR.

Finally, we believe that the largest source of difference in our results relative to Bird et al. (2013) is due to the fact that Bird et al. identified MAPs with a much larger age range. In this work, single stellar populations span a very narrow range in formation time ($\Delta t_{form} = 50$ Myr); the specific formation time ranges are chosen such that any MAP forms just prior to a recorded simulation output (i.e. an epoch that was written to disc). The oldest stars included in the σ_{birth} measurements are therefore 50 Myr old, at maximum. In contrast, Bird et al. (2013) define cohorts with $\Delta t_{form} \gtrsim 1$ Gyr. Dynamical heating is typically strongest right after birth (see Fig. 2). Thus, the Δt_{form} used in Bird et al. is likely to have increased σ_{birth} from its true *in-situ* value. We note that the main results of Bird et al. (2013) are not changed by this realization; the *in-situ* kinematics of stars at birth still evolved with formation time and had a significant impact on the present-day kinematics of each cohort.

To ensure that the present analysis was not affected in a similar manner, we experimented with even smaller ranges of formation time and found no decrease in σ_{birth} for populations as young as 0.5 Myr. We are therefore confident that the σ_{birth} values reported here truly reflect the *in-situ* kinematics of each MAP, and that we have accurately captured the subsequent heating of these populations soon after birth.

4.3 Connection to high z discs

The equilibrium disc model that we have shown reproduces the evolution of σ_{birth} for stars in h277 (Fig. 5) has also been shown to reproduce the AVR in Local Group galaxies (Leaman et al. 2017), as well as the evolution in $\sigma(z)$ seen in disc galaxies (e.g. Swinbank et al. 2012; Wisnioski et al. 2015; Turner et al. 2017; Übler et al. 2019). This model tracks the mid-plane pressure, which is correlated with $\dot{\Sigma}_\star$. In this model, dependence of σ_{birth} on position (Fig. 4) is expected at late times. Observations of resolved, nearby galaxies find negative radial gradients in both the atomic and molecular gas velocity dispersion (Tamburro et al. 2009). At a fixed epoch, σ_{birth} should decrease with increasing radius if the mid-plane surface density decreases with radius and stars are born in hydrostatic equilibrium. Similarly, σ_{birth} should increase with z as f_{gas} increases, and the kinematics of newly forming stars is thus a function of both position and time within the disc. This not only has important implications for observations of resolved stellar kinematics in the MW and local galaxies (Leaman et al. 2017), but also for the kinematic evolution of disc galaxies out to $z \sim 2$.

The observed decrease in the gas velocity dispersion of disc galaxies with decreasing z has been dubbed 'disc settling.' Wisnioski et al. (2015) demonstrated that disc settling could be explained within a model wherein the velocity dispersion of gas evolves according to the gas fraction within a stable disc. Upside-down growth is consistent with disc settling and implies that it is an

evolutionary sequence traversed not just by the population, but by individual galaxies as well. In fact, Kassin et al. (2014) analysed h277 (along with three other Milky Way-mass galaxies run with the same physics) and found that the global gas velocity dispersion, σ_g, in the simulations decreases with time. They found that the slope of the $\sigma_g(z)$ evolution for the simulated galaxies is consistent with observed evolution, though they were unable to match the normalization of $\sigma_g(z)$ due to the difficulty of identifying gas in the simulations that is a proper match to the star formation-heated gas that observers use as a tracer. Despite showing that these galaxies match the observed evolution, Kassin et al. (2014) did not explore the origin of the evolution. The results in this work explain the Kassin et al. result in light of the same models applied to explain observed disc settling. The settling of the disc in h277 appears to be strongly linked to the evolving SFR balanced by the supply of gas for star formation.

5 CONCLUSIONS

We find the solar neighbourhood AVR measured in h277 is nearly identical to that in the MW. To the best of our knowledge, this is the first cosmological zoom-in MW-mass simulation to recover the low velocity dispersions expected of molecular gas at $z = 0$, and stars in the simulation are then born with these low dispersions. The velocity dispersion of the star-forming gas in h277 is ~ 6 km s^{-1} at $z = 0$ in the simulated solar neighbourhood (Fig. 3). Typically, the velocity dispersion of the star-forming gas reservoir stays > 10 km s^{-1} in cosmological zoom-in simulations, even of MW-like galaxies (e.g. Bird et al. 2013; Minchev et al. 2013; Roškar et al. 2013; Martig et al. 2014; Buck et al. 2020; Sanderson et al. 2020). The detailed AVR arose self-consistently from the formation and dynamical evolution of h277. It is therefore interesting to analyse how the AVR came about. Through a combination of upside-down and inside-out formation, the resulting AVR yields an excellent match to the MW AVR for stellar populations through > 10 Gyr old.

There has been a lot of debate about the relative influence of dynamical evolution on stars in the solar neighbourhood. In this work, we examine the kinematics of stars in the simulated solar neighbourhood, including at their birth and their subsequent evolution, in order to understand how the present-day AVR of the solar neighbourhood came to be. In addition, we consider as a whole the simulated galactic disc at high redshift. This analysis allows us to draw comparisons between the vertical disc dynamics observed at $z = 0$ and observed dynamics in MW proxies observed at high z.

Although this is just a single simulated galaxy, h277 has managed to reproduce a number of observed trends in disc galaxy evolution. In this work, we have shown

(i) The radius of the star-forming disc in h277 grows with time (inside-out, Fig. 5), and σ_{birth} decreases with time. At any given time, σ_{birth} depends on radius. At any given radius, σ_{birth} depends on time, consistent with an upside-down formation in which the disc cools or settles with time. Thus, σ_{birth} is a function of both formation time and formation radius within the disc, and is strongly correlated with $\dot{\Sigma}_\star$ (Fig. 4).

(ii) The oldest stars in the solar neighbourhood in h277 were born at smaller radii (Fig. 3), but contribute to the $z = 0$ AVR due to radial mixing. On the other hand, the youngest stars in the solar neighbourhood tend to be born locally. Given the dependence of σ_{birth} on time and radius, radial mixing tends to amplify the σ_{birth} evolution with age seen in the outer disc and specifically at the solar neighbourhood.

(iii) Mono-age stellar populations are also kinematically heated after birth (Fig. 2). While we have not directly explored the origin of the heating in this paper, the ability of this simulation to capture the clumpy ISM suggests that scattering off of GMCs after birth contributes to the heating, and this hypothesis is consistent with the measured heating rate. Given that h277 has a very quiescent merger history, mergers are not likely to play a role in this heating.

(iv) One of the key criteria necessary to match the MW's observed AVR is the ability to form stars with a low velocity dispersion, σ_{birth}, in order to match the low velocity dispersions seen in young stars in the MW. This simulation follows the non-equilibrium formation and destruction of molecular hydrogen H_2 gas, and ensures that stars form only in the presence of H_2 (Christensen et al. 2012). Importantly, the stars are then born with this low dispersion, and not prone to processes that can introduce additional sources of dispersion at birth, such as star formation in outflowing gas (El-Badry et al. 2016). The ability to model cold gas velocity dispersions is also what allows the upside-down disc formation, as well as subsequent heating, to emerge.

(v) Not only does h277 match the local observations of the Milky Way, but its evolution is also completely consistent with observations that show that discs were kinematically hotter in the past and have 'settled' with time. We have shown that a model that has been invoked to explain disc settling (Wisnioski et al. 2015), in which the disc evolves in quasi-equilibrium and the velocity dispersion of the gas is tied to the evolving gas fraction inside disc galaxies, can match the evolution of σ_{birth} seen in h277 (Fig. 5). Thus, the equilibrium model can explain both the populations of disc galaxies with time, and the evolution of this individual galaxy.

h277 is just one simulation of a Milky Way-mass galaxy, so it is not yet clear if the results will persist in additional simulations. However, Kassin et al. (2014) showed that four simulated galaxies, including h277, matched the declining gas velocity dispersion witnessed over time in galaxy discs, suggesting that other galaxies may show similar trends. In future work, we will explore a larger range of merger histories to discover if the match to the MW AVR can hold in a less quiescent galaxy.

The correlation between σ_{birth} and $\dot{\Sigma}_{\star}$ across both spatial position and time noted in this work (Fig. 4) is expected for galaxies on the star-forming main sequence and generically predicts upside-down disc formation. Most theoretical models of star formation – marginal gas disc stability including self-gravity considerations (e.g. Toomre 1964), feedback-driven turbulence (e.g. Faucher-Giguère et al. 2013), and accretion powered turbulence (e.g. Krumholz et al. 2018) – ultimately predict a correlation between gas velocity dispersion and $\dot{\Sigma}_{\star}$. If these models capture reality, the velocity dispersion of the star-forming gas reservoir will decrease with time in a galaxy with a declining SFH, just as in h277. If $\dot{\Sigma}_{\star}$ has a negative radial gradient, then σ_{birth} will decrease with time even for an unchanging SFR. As the galaxy grows inside-out, the characteristic radius of the star-forming disc moves outwards to lower $\dot{\Sigma}_{\star}$ and thus lower σ_{birth}.

Additionally, we have shown in this work that a quasi-stable model for h277's disc can predict the evolution in σ_{birth} seen in the simulation, but we have not fully verified that the model describes the simulation's underlying physics. In a future work, we will test the equilibrium of h277's disc. We will also explore the heating mechanism of stars after birth, and use the kinematics of simulated stars (e.g. the shape of the velocity ellipsoid) to interpret whether similar mechanisms might have been at play in shaping the Milky Way's AVR.

DATA AVAILABILITY

The data underlying this article are available in EUDAT, at http://doi.org/10.23728/b2share.c4ac776194a043f6ba8c6fa1e7719d08.

REFERENCES

Agertz O., Lake G., Teyssier R., Moore B., Mayer L., Romeo A. B., 2009, MNRAS, 392, 294
Agertz O., Kravtsov A. V., Leitner S. N., Gnedin N. Y., 2013, ApJ, 770, 25
Astropy Collaboration, 2013, A&A, 558, A33
Astropy Collaboration, 2018, AJ, 156, 123
Aumer M., Binney J., Schönrich R., 2016, MNRAS, 462, 1697
Barnes K. L., van Zee L., Dale D. A., Staudaher S., Bullock J. S., Calzetti D., Chandar R., Dalcanton J. J., 2014, ApJ, 789, 126
Beasley M. A., San Roman I., Gallart C., Sarajedini A., Aparicio A., 2015, MNRAS, 451, 3400
Beers T. C., Flynn K., Gebhardt K., 1990, AJ, 100, 32
Belokurov V., Erkal D., Evans N. W., Koposov S. E., Deason A. J., 2018, MNRAS, 478, 611
Benincasa S. M., Wadsley J., Couchman H. M. P., Keller B. W., 2016, MNRAS, 462, 3053
Bhattacharya S., et al., 2019, A&A, 631, A56
Binney J., Tremaine S., 2008, Galactic Dynamics: Second Edition. Princeton Univ. Press, Princeton
Bird J. C., Kazantzidis S., Weinberg D. H., Guedes J., Callegari S., Mayer L., Madau P., 2013, ApJ, 773, 43
Bland-Hawthorn J., Gerhard O., 2016, ARA&A, 54, 529
Boardman N., et al., 2020, MNRAS, 491, 3672
Bournaud F., Elmegreen B. G., 2009, ApJ, 694, L158
Bournaud F., Elmegreen B. G., Martig M., 2009, ApJ, 707, L1
Bovy J., Rix H.-W., 2013, ApJ, 779, 115
Brook C. B., et al., 2012, MNRAS, 426, 690
Brook C. B., Kawata D., Gibson B. K., Freeman K. C., 2004, ApJ, 612, 894
Brooks A. M., Zolotov A., 2014, ApJ, 786, 87
Brooks A. M., Papastergis E., Christensen C. R., Governato F., Stilp A., Quinn T. R., Wadsley J., 2017, ApJ, 850, 97
Bryan G. L., Norman M. L., 1998, ApJ, 495, 80
Bryant J. J., et al., 2015, MNRAS, 447, 2857
Buck T., Obreja A., Macciò A. V., Minchev I., Dutton A. A., Ostriker J. P., 2020, MNRAS, 491, 3461
Bundy K., et al., 2015, ApJ, 798, 7
Carlberg R. G., Sellwood J. A., 1985, ApJ, 292, 79

---

[9] http://www.astropy.org

Casagrande L., Schönrich R., Asplund M., Cassisi S., Ramírez I., Meléndez J., Bensby T., Feltzing S., 2011, A&A, 530, A138

Ceverino D., Primack J., Dekel A., Kassin S. A., 2017, MNRAS, 467, 2664

Christensen C., Quinn T., Governato F., Stilp A., Shen S., Wadsley J., 2012, MNRAS, 425, 3058

Christensen C. R., Governato F., Quinn T., Brooks A. M., Shen S., McCleary J., Fisher D. B., Wadsley J., 2014, MNRAS, 440, 2843

Christensen C. R., Davé R., Governato F., Pontzen A., Brooks A., Munshi F., Quinn T., Wadsley J., 2016, ApJ, 824, 57

Contini T., et al., 2016, A&A, 591, A49

Daddi E., et al., 2010, ApJ, 713, 686

Davé R., Finlator K., Oppenheimer B. D., 2012, MNRAS, 421, 98

Dekel A., Mandelker N., 2014, MNRAS, 444, 2071

Dorman C. E., et al., 2015, ApJ, 803, 24

Dutton A. A., Macciò A. V., Buck T., Dixon K. L., Blank M., Obreja A., 2019, MNRAS, 486, 655

El-Badry K., Wetzel A., Geha M., Hopkins P. F., Kereš D., Chan T. K., Faucher-Giguère C.-A., 2016, ApJ, 820, 131

Epinat B., et al., 2009, A&A, 504, 789

Fall S. M., Efstathiou G., 1980, MNRAS, 193, 189

Faucher-Giguère C.-A., Quataert E., Hopkins P. F., 2013, MNRAS, 433, 1970

Flores H., Hammer F., Puech M., Amram P., Balkowski C., 2006, A&A, 455, 107

Forbes J. C., Krumholz M. R., Burkert A., Dekel A., 2014, MNRAS, 438, 1552

Förster Schreiber N. M., et al., 2009, ApJ, 706, 1364

Frankel N., Rix H.-W., Ting Y.-S., Ness M., Hogg D. W., 2018, ApJ, 865, 96

Frankel N., Sanders J., Rix H.-W., Ting Y.-S., Ness M., 2019, ApJ, 884, 99

Genzel R., et al., 2006, Nature, 442, 786

Genzel R., et al., 2011, ApJ, 733, 101

Gill S. P. D., Knebe A., Gibson B. K., 2004, MNRAS, 351, 399

Glazebrook K., 2013, Publ. Astron. Soc. Aust., 30, e056

Gnerucci A., et al., 2011, A&A, 528, A88

Gogarten S. M., et al., 2010, ApJ, 712, 858

Governato F., et al., 2010, Nature, 463, 203

Governato F., et al., 2012, MNRAS, 422, 1231

Grand R. J. J., Springel V., Gómez F. A., Marinacci F., Pakmor R., Campbell D. J. R., Jenkins A., 2016, MNRAS, 459, 199

Green A. W., et al., 2014, MNRAS, 437, 1070

Gustafsson B., Church R. P., Davies M. B., Rickman H., 2016, A&A, 593, A85

Haardt F., Madau P., 2001, in Neumann D. M., Tran J. T. V., eds, Clusters of Galaxies and the High Redshift Universe Observed in X-rays, preprint, (astro-ph/0106018).

Hirtenstein J., et al., 2019, ApJ, 880, 54

Holmberg J., Nordström B., Andersen J., 2009, A&A, 501, 941

Hopkins P. F., et al., 2018, MNRAS, 480, 800

House E. L., et al., 2011, MNRAS, 415, 2652

Hu S., Sijacki D., 2018, MNRAS, 478, 1576

Hung C.-L., et al., 2019, MNRAS, 482, 5125

Ida S., Kokubo E., Makino J., 1993, MNRAS, 263, 875

Jenkins A., Binney J., 1990, MNRAS, 245, 305

Jones T. A., Swinbank A. M., Ellis R. S., Richard J., Stark D. P., 2010, MNRAS, 404, 1247

Jonsson P., 2006, MNRAS, 372, 2

Kassin S. A., et al., 2012, ApJ, 758, 106

Kassin S. A., Brooks A., Governato F., Weiner B. J., Gardner J. P., 2014, ApJ, 790, 89

Katz N., White S. D. M., 1993, ApJ, 412, 455

Kennicutt Robert C. J., 1998, ApJ, 498, 541

Kim C.-G., Ostriker E. C., Kim W.-T., 2013, ApJ, 776, 1

Knollmann S. R., Knebe A., 2009, ApJS, 182, 608

Koyama H., Ostriker E. C., 2009, ApJ, 693, 1346

Krumholz M. R., Burkhart B., 2016, MNRAS, 458, 1671

Krumholz M. R., Dekel A., McKee C. F., 2012, ApJ, 745, 69

Krumholz M. R., Burkhart B., Forbes J. C., Crocker R. M., 2018, MNRAS, 477, 2716

Kuhn M. A., Hillenbrand L. A., Sills A., Feigelson E. D., Getman K. V., 2019, ApJ, 870, 32

Kumamoto J., Baba J., Saitoh T. R., 2017, PASJ, 69, 32

Lacey C. G., 1984, MNRAS, 208, 687

Law D. R., Steidel C. C., Erb D. K., Larkin J. E., Pettini M., Shapley A. E., Wright S. A., 2009, ApJ, 697, 2057

Leaman R., et al., 2017, MNRAS, 472, 1879

Lehnert M. D., Di Matteo P., Haywood M., Snaith O. N., 2014, ApJ, 789, L30

Lemoine-Busserolle M., Bunker A., Lamareille F., Kissler-Patig M., 2010, MNRAS, 401, 1657

Leroy A. K., Walter F., Brinks E., Bigiel F., de Blok W. J. G., Madore B., Thornley M. D., 2008, AJ, 136, 2782

Leroy A. K., et al., 2016, ApJ, 831, 16

Loebman S. R., Roškar R., Debattista V. P., Ivezić, Ž., Quinn T. R., Wadsley J., 2011, ApJ, 737, 8

Loebman S. R., Ivezić Ž., Quinn T. R., Governato F., Brooks A. M., Christensen C. R., Jurić M., 2012, ApJ, 758, L23

Loebman S. R., et al., 2014, ApJ, 794, 151

Ma X., Hopkins P. F., Wetzel A. R., Kirby E. N., Anglés-Alcázar D., Faucher-Giguère C.-A., Kereš D., Quataert E., 2017, MNRAS, 467, 2430

Mackereth J. T., et al., 2019, MNRAS, 489, 176

Martig M., Minchev I., Flynn C., 2014, MNRAS, 443, 2452

Mason C. A., et al., 2017, ApJ, 838, 14

Mieda E., Wright S. A., Larkin J. E., Armus L., Juneau S., Salim S., Murray N., 2016, ApJ, 831, 78

Minchev I., Quillen A. C., 2006, MNRAS, 368, 623

Minchev I., Chiappini C., Martig M., 2013, A&A, 558, A9

Munshi F., et al., 2013, ApJ, 766, 56

Nestingen-Palm D., Stanimirović S., González-Casanova D. F., Babler B., Jameson K., Bolatto A., 2017, ApJ, 845, 53

Nordström B., et al., 2004, A&A, 418, 989

Orr M. E., et al., 2018, MNRAS, 478, 3653

Orr M. E., Hayward C. C., Hopkins P. F., 2019, MNRAS, 486, 4724

Orr M. E., et al., 2020, MNRAS, 496, 1620

Peng C. Y., Ho L. C., Impey C. D., Rix H.-W., 2010, AJ, 139, 2097

Peterken T., Merrifield M., Aragón-Salamanca A., Fraser-McKelvie A., Avila-Reese V., Riffel R., Knapen J., Drory N., 2020, MNRAS, 495, 3387

Pontzen A., Roškar R., Stinson G., Woods R., 2013, pynbody: N-Body/SPH analysis for python, record ascl:1305.002

Popping G., et al., 2015, MNRAS, 454, 2258

Quinn P. J., Hernquist L., Fullagar D. P., 1993, ApJ, 403, 74

Romeo A. B., Falstad N., 2013, MNRAS, 433, 1389

Romeo A. B., Wiegert J., 2011, MNRAS, 416, 1191

Roškar R., Debattista V. P., Stinson G. S., Quinn T. R., Kaufmann T., Wadsley J., 2008, ApJ, 675, L65

Roškar R., Debattista V. P., Brooks A. M., Quinn T. R., Brook C. B., Governato F., Dalcanton J. J., Wadsley J., 2010, MNRAS, 408, 783

Roškar R., Debattista V. P., Loebman S. R., 2013, MNRAS, 433, 976

Ruchti G. R., et al., 2015, MNRAS, 450, 2874

Sanders J. L., Das P., 2018, MNRAS, 481, 4093

Sanderson R. E., et al., 2020, ApJS, 246, 6

Schmidt M., 1959, ApJ, 129, 243

Sellwood J. A., 2008, in Funes J. G., Corsini E. M., eds, ASP Conf. Ser. Vol. 396, Formation and Evolution of Galaxy Disks. Astron. Soc. Pac., San Francisco, p. 341

Sellwood J. A., 2014, Rev. Mod. Phys., 86, 1

Sellwood J. A., Binney J. J., 2002, MNRAS, 336, 785

Semenov V. A., Kravtsov A. V., Gnedin N. Y., 2016, ApJ, 826, 200

Semenov V. A., Kravtsov A. V., Gnedin N. Y., 2018, ApJ, 861, 4

Shen S., Wadsley J., Stinson G., 2010, MNRAS, 407, 1581

Simons R. C., et al., 2016, ApJ, 830, 14

Snaith O., Haywood M., Di Matteo P., Lehnert M. D., Combes F., Katz D., Gómez A., 2015, A&A, 578, A87

Spergel D. N., et al., 2003, ApJS, 148, 175

Spitzer L., Jr, Schwarzschild M., 1951, ApJ, 114, 385

Stark A. A., Brand J., 1989, ApJ, 339, 763

Stilp A. M., Dalcanton J. J., Skillman E., Warren S. R., Ott J., Koribalski B., 2013, ApJ, 773, 88

Stinson G., Seth A., Katz N., Wadsley J., Governato F., Quinn T., 2006, MNRAS, 373, 1074

Stott J. P., et al., 2016, MNRAS, 457, 1888

Sun J., et al., 2020, ApJ, 892, 148

Swinbank A. M., Smail I., Sobral D., Theuns T., Best P. N., Geach J. E., 2012, ApJ, 760, 130

Tacconi L. J., et al., 2013, ApJ, 768, 74

Tamburro D., Rix H. W., Leroy A. K., Mac Low M. M., Walter F., Kennicutt R. C., Brinks E., de Blok W. J. G., 2009, AJ, 137, 4424

Thompson T. A., Quataert E., Murray N., 2005, ApJ, 630, 167

Ting Y.-S., Rix H.-W., 2019, ApJ, 878, 21

Ting Y.-S., Hawkins K., Rix H.-W., 2018, ApJ, 858, L7

Toomre A., 1964, ApJ, 139, 1217

Toth G., Ostriker J. P., 1992, ApJ, 389, 5

Turner O. J., et al., 2017, MNRAS, 471, 1280

Villumsen J. V., 1985, ApJ, 290, 75

Wadsley J. W., Stadel J., Quinn T., 2004, New Astron., 9, 137

White S. D. M., Rees M. J., 1978, MNRAS, 183, 341

Wielen R., 1977, A&A, 60, 263

Wiklind T., et al., 2019, ApJ, 878, 83

Williams B. F., Dalcanton J. J., Dolphin A. E., Holtzman J., Sarajedini A., 2009, ApJ, 695, L15

Wilson C. D., et al., 2011, MNRAS, 410, 1409

Wisnioski E., et al., 2015, ApJ, 799, 209

Wisnioski E., et al., 2019, ApJ, 886, 124

Yu X., et al., 2019, MNRAS, 486, 4463

Yu J., Liu C., 2018, MNRAS, 475, 1093

Zolotov A., et al., 2012, ApJ, 761, 71

Übler H., et al., 2019, ApJ, 880, 48

This paper has been typeset from a TeX/LaTeX file prepared by the author.